

Original Research Article

Thermoelectric study of $\text{La}_2\text{Ti}_{2-x}\text{Nb}_x\text{O}_7$ ($0 \leq x \leq 0.25$) ceramic materials

ABSTRACT

$\text{La}_2\text{Ti}_{2-x}\text{Nb}_x\text{O}_7$ ($x = 0.00, 0.05, 0.10, 0.15, 0.20, 0.25$) powders were synthesised via solid state reaction method, followed by sintering at 1673 K in a reducing atmosphere of 5% H_2/N_2 gas. The crystal structure, microstructure and thermoelectric (TE) properties of the pure and Nb-doped $\text{La}_2\text{Ti}_2\text{O}_7$ ceramics were investigated. All compositions were single phase with porous microstructures consistent with their low experimental densities. Thermoelectric results of Nb-doped compositions showed improved properties in comparison to pure $\text{La}_2\text{Ti}_2\text{O}_7$, suggesting that cation doping has the potential to improve the thermoelectric properties. Generally, the TE results obtained are not suitable for thermoelectric applications. However, the high Seebeck coefficient ($\geq 190 \mu\text{V/K}$) and glass-like thermal conductivity ($\leq 2.26 \text{ W/m.K}$) values achieved have opened a new window for exploring the thermoelectric potentials of $\text{La}_2\text{Ti}_2\text{O}_7$ and other related oxides.

Keywords: Solid state reaction, thermoelectric, seebeck coefficient, thermal conductivity, $\text{La}_2\text{Ti}_2\text{O}_7$

1. INTRODUCTION

Thermoelectric generators (TEGs) are solid state devices that convert a heat flux directly into electrical power [1]. The performance of TEGs is controlled by two main factors: functionality and efficiency of the semiconducting materials (thermoelements) from which the generator is composed. The functionality is based on a heavily doped p-type and n-type semiconducting materials with a high carrier concentration, n ($n \sim 10^9\text{-}10^{21} \text{ cm}^{-3}$) [2] and a bandgap of $\sim 10 \text{ K}_B T$ [3] connected electrically in series and thermally in parallel. The efficiency depends on the dimensionless figure of merit, ZT represented as:

$$ZT = \frac{S^2 \sigma T}{k}$$

(1)

where S is the Seebeck coefficient, σ is the electrical conductivity, T is the absolute temperature and $k = k_L + k_E$ [4] is the total thermal conductivity. k_L and k_E are lattice thermal conductivity (thermal contributions from lattice vibrations/phonons) and electronic thermal conductivity (thermal contributions from charge carriers), respectively.

Non-oxide alloys such as $\text{Bi}_2\text{T}_3/\text{Se}_3$, Sb_2Te_3 , PbTe/Se and SiGe [5] presently are the most studied thermoelectric semiconducting materials. Due to their framework structures consisting of large voids with heavy elements, they possess low phonon group velocity and thus low k which are desirable for optimised ZT [6]. Application of these materials is limited, however, due to toxicity, scarcity, cost and limited operational temperature range [7]. According to Ioffe's theory, oxides are unsuitable for TE applications owing to their strong, mixed ionic and covalent bonds, high k_L and lower carrier mobilities resulting in low electrical conductivity [8]. Conversely, there is strong evidence that oxide thermoelectrics containing transition-metal-oxides are novel alternative materials to the conventional TE materials. Oxides are inert, non-toxic, light weight, cheap, possess small thermal expansion with high melting temperature, hence promising TE candidates for high temperature applications [9-11].

The study of electrical properties of lanthanum dititanate, $\text{La}_2\text{Ti}_2\text{O}_7$ (LTO) ferroelectrics started over thirty years ago [12]. LTO belongs to the perovskite-like layered structure family with a homologous series $\text{A}_n\text{B}_n\text{O}_{3n+2}$, where A = rare earth (RE) elements, B = titanium and n ($= 4$ in this case of LTO) is the number of octahedral units in the perovskite layers [13, 14]. At room temperature, LTO possesses a monoclinic unit cell with a space group of P21 and a corresponding lattice parameter $a = 13.0150 \text{ \AA}$, $b = 5.5456 \text{ \AA}$, $c = 7.8170 \text{ \AA}$ and $\beta = 98.6^\circ$ [14]. Above room temperature, LTO undergoes a transformation. For instance, at $\sim 780 \text{ }^\circ\text{C}$, it transforms to orthorhombic phase (CMc21) and changes to a paraelectric phase (CMcm) at $1500 \text{ }^\circ\text{C}$ [12, 15]. $\text{La}_2\text{Ti}_2\text{O}_7$ exhibits high curie temperature, $T_c > 1500 \text{ }^\circ\text{C}$ [12, 13, 15], excellent piezoelectric properties [12, 13, 16], non-linear optical and photocatalytic properties [12, 13, 15, 16] and finds application in gas turbines at high temperature ($> 1000 \text{ }^\circ\text{C}$) [15].

The structure of LTO consists of discontinuous layers of corner sharing TiO_6 octahedra in the unit cell [13, 14] with La occupying interstitial positions between the octahedral (Figure 1) [13]. Pure LTO has a wide bandgap (E_g) of 3 - 4 eV [17, 18]. The size of E_g is dependent on the microstructure [17], morphology [18] and processing method of $\text{La}_2\text{Ti}_2\text{O}_7$ [18].

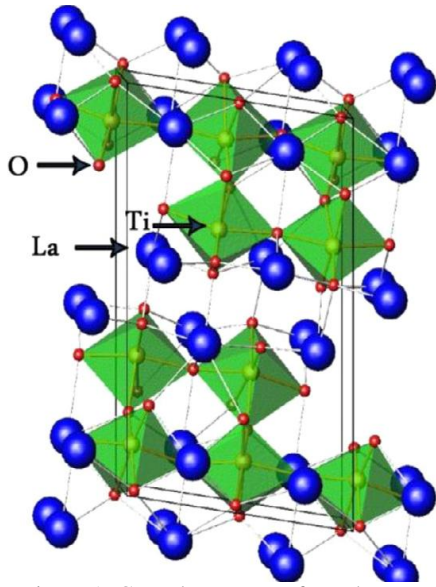


Figure 1. Crystal structure of Lanthanum dititanate, $\text{La}_2\text{Ti}_2\text{O}_7$ [13]. Blue, red, and green balls correspond to La^{3+} , O^{2-} and Ti^{4+} ions, respectively.

The thermoelectric properties of LTO and other related layered perovskites have received less attention. Recently, Kholiq *et al* [14] reported a low thermal conductivity value ($k \sim 1.3 \text{ W/m.K}$) at 573 K in pure $\text{La}_2\text{Ti}_2\text{O}_7$, and very low values of ~ 1.12 and $\sim 0.93 \text{ W/m.K}$ for Sr- and Ta-doped $\text{La}_2\text{Ti}_2\text{O}_7$, respectively at 573 K. These low k values are attributed to its large unit cells, large atomic mass, crystal anisotropy and complex crystal structure. As a complex structural material, it shows a high flexibility for tuning through cation/anion substitution which together with intrinsic low k are vital constituents required for a thermoelectric material.

2. MATERIALS AND METHOD

Ceramic compositions of $\text{La}_2\text{Ti}_{2-x}\text{Nb}_x\text{O}_7$ ($0 \leq x \leq 0.25$) were prepared by solid state reaction (SSR) method from the following starting powders: La_2O_3 (99.99 %, Sigma-Aldrich, UK), TiO_2 (99.90 %, Sigma-Aldrich, UK) and Nb_2O_5 (99.50 %, Stanford Materials Corporation, USA). The raw powders (La_2O_3 , TiO_2 and Nb_2O_5) were dried in a clean chamber furnace at $900 \text{ }^\circ\text{C}$ for 8 h and cooled to $200 \text{ }^\circ\text{C}$. All dried powders were transferred to a vacuum desiccator and allowed to cool to room temperature in order to prevent adsorption of moisture. Stoichiometric proportions of the dried powders were mixed by ball milling in isopropanol with yttria stabilised zirconia (YSZ) milling media for 24 h. the slurry was dried at $80 \text{ }^\circ\text{C}$, sieved through a $250 \text{ }\mu\text{m}$ mesh and calcined

at 1573 K in air for 6 h using alumina crucible [19]. The calcined powders were ground and pressed into a disc (20 mm diameter, ≤ 2 mm thickness) pellet in a uniaxial press. The green pellets were sintered in flowing 5% H₂/N₂ gas at 1673 K for 6 h.

Crystal structures of the ceramics were characterised by powder x-ray diffraction (XRD) with Cu K α radiation ($\lambda = 1.5406$ Å) using D2 phaser diffractometer (Bruker AX GmbH, Germany). The scan was conducted across the 2θ range of 20-60 degrees with a step size of 0.01° at a scan rate of $1^\circ/\text{min}$. Phase identity and purity of the collected data were analysed using the ICDD SLeve+PDF-4+ software [20]. Prior to microstructural examination, samples were ground, polished, thermally etched and carbon coated. Microstructures of the samples were studied using Philips XL 30 S-FEG scanning electron microscope.

Seebeck coefficient and electrical conductivity of disc samples were measured simultaneously in the temperature range of 573-973 K in an argon gas atmosphere using a Netzch SBA 458 Nemesis Seebeck and electrical conductivity analyser. Thermal properties (thermal diffusivity λ , specific heat capacity C_p and thermal conductivity k) were measured on 10 x 10 mm square samples using a thermal properties analyser (Anter Flashline TM 3000) with a high speed xenon discharge (HSXD) pulse source [21]. The experimental density of the ceramics was determined by Archimedes method using an electronic digital density balance (Mettler-Toledo AG balance).

3. RESULTS AND DISCUSSION

The room temperature XRD patterns of La₂Ti_{2-x}Nb_xO₇ (LTO) ceramics are shown in Figure 2(a). The patterns are indexed to a La₂Ti₂O₇ monoclinic structure ceramic (space group, P2₁) with the lattice constant $a = 7.80896(10)$ Å, $b = 5.54608(7)$ Å, and $c = 13.01425(22)$ Å, [22] consistent with those reported in the literature [14, 15]. No secondary phases were detected in any of the compositions within the detection limit of the diffractometer, and the peaks were sharp, suggesting a large particle size according to the Scherrer formula [14]. The bulk and relative density of all compositions for different Nb concentrations are plotted in Figure 2(b). The relative density of all compositions varied progressively from 84 % to 93 %. This implies the bulk density increased with increase in Nb concentration with $x = 0.25$ showing the maximum sintering density of 5.38 g/cm^3 (93 % of theoretical density, 5.789 g/cm^3) [22].

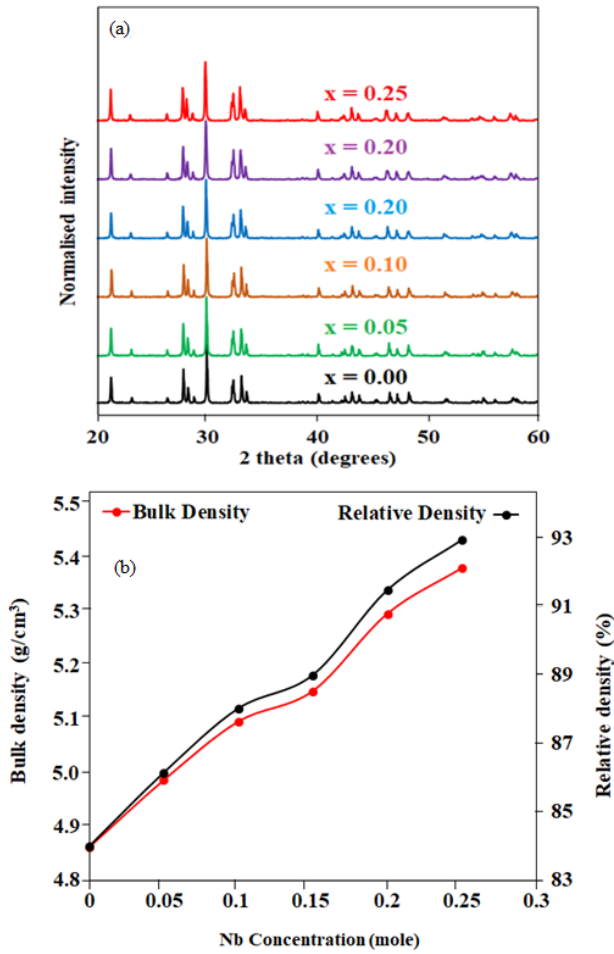


Figure 2. XRD patterns of $\text{La}_2\text{Ti}_{2-x}\text{Nb}_x\text{O}_7$ (LTO) ceramics (a) and the Archimedes measured density (b). The uncertainty in density measurement is $\pm 0.05\%$.

The SEM images of the 5% H_2/N_2 sintered, thermally etched and carbon coated surfaces for $\text{La}_2\text{Ti}_{2-x}\text{Nb}_x\text{O}_7$; $0.00 \leq x \leq 0.25$ ceramics are shown in Figure 3. The SEM images revealed homogenous and porous structures consistent with their low relative density of $\leq 93\%$ and average grain size of $\leq 2\ \mu\text{m}$. The effect of porosity on the thermoelectric performance of these compositions is unclear. However, some authors have suggested the presence of porosity in the lattice creates discontinuities which act as scattering centres thereby restricting carrier mobility and enhancing phonon scattering [21, 23, 24]. As a result, both electrical conductivity, σ and thermal conductivity, k is reduced.

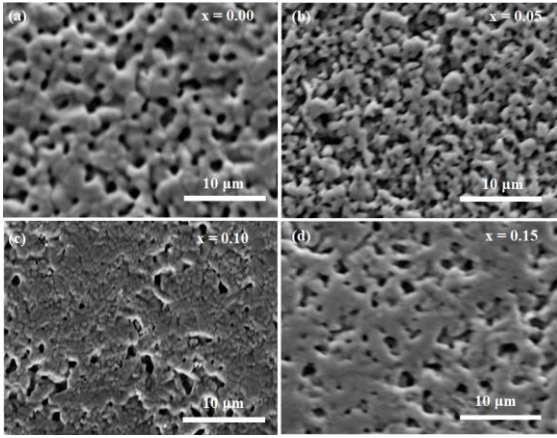


Figure 3. SEM micrographs of the surfaces for $\text{La}_2\text{Ti}_{2-x}\text{Nb}_x\text{O}_7$ ($0.00 \leq x \leq 0.25$) ceramics sintered 6 hours in 5% H_2/N_2 at 1773 K.

Figures 4 and 5 show the temperature dependence of the electrical conductivity (σ), absolute Seebeck coefficient ($|S|$), power factor (PF), respectively for $\text{La}_2\text{Ti}_{2-x}\text{Nb}_x\text{O}_7$ ceramic compositions. $x = 0.00$ (undoped $\text{La}_2\text{Ti}_2\text{O}_7$) exhibited the lowest σ in all the measured temperature range, consistent with its lowest density (Figure 2b). The low σ obtained in $x = 0.00$ showed that carrier mobility was restricted probably by the inherent heavy pores in the grains. The electrical conductivity increased with Nb doping but inconsistent with dopant (Nb) concentration. $x = 0.10$ showed the highest σ in all the measured temperature range (Figure 4a), reaching a maximum of ~ 2.0 S/cm (200 S/m) at 873 K. This increase in electrical conductivity is attributed to the increase in carrier (electron) concentration due to the substitution of Nb^{5+} for Ti^{4+} which produces electrons. Moreover, oxygen vacancy, V_{O} introduced by processing in reducing atmosphere increases the carrier concentration, thereby increasing σ [25, 26]. Some authors have also suggested the effect of grain size as a contributory factor to the enhanced σ . Doping has generally been observed to increase grain size, resulting in a reduced grain boundary area and scattering which may enhance the conduction [25-27]. The highest σ (200 S/m) at 873 K for $\text{La}_2\text{Ti}_{1.9}\text{Nb}_{0.1}\text{O}_7$ obtained in this study is higher than the maximum σ (0.5 S/m) reported in the literature for $\text{La}_{1.6}\text{Sr}_{0.4}\text{Ti}_2\text{O}_{6.8\pm\delta}$ ceramic at 573 K [14].

Figure 4(b) shows the Seebeck coefficient, $|S|$ of $\text{La}_2\text{Ti}_{2-x}\text{Nb}_x\text{O}_7$ sample as a function of temperature. S of all ceramics are negative, indicating that electrons are the dominant carriers [26, 28-30]. S increased monotonically with increasing temperature in all the measured temperature range.

However, the behaviour of S of the sample is inconsistent with Ioffe theory [31] (except $x = 0.00$ at 973 K). The relationship between S and carrier concentration is given by the following equation [28]:

$$S = \gamma + \ln \frac{1}{n}$$

(2)

where γ and n are the scattering factor and the carrier concentration, respectively. S is inversely proportional to the carrier concentration. This implies that $x = 0.00$ with the lowest σ (lowest carrier concentration) is expected to show the highest S in all temperatures while $x = 0.10$ should likewise exhibit the lowest S as a result its high σ in obedience with Ioffe's theory. At the maximum measured temperature (973 K), $x = 0.00$ as expected exhibited the highest absolute Seebeck coefficient value of $\sim 389 \mu\text{V/K}$. This value is larger than values obtainable in most doped SrTiO_3 ceramics in the literature [28, 32-35].

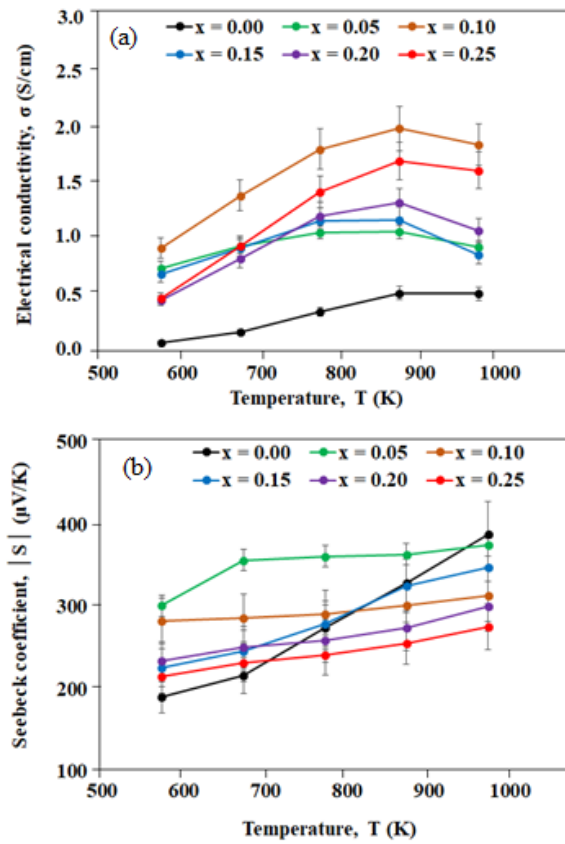


Figure 4. Temperature dependence of electrical conductivity (a) and Seebeck coefficient (b) for pure and Nb-doped $\text{La}_2\text{Ti}_2\text{O}_7$ ceramics sintered 6 hours in 5% H_2/N_2 at 1773 K.

Combining the electrical conductivity and the Seebeck coefficient, the power factor (PF) of $\text{La}_2\text{Ti}_{2-x}\text{Nb}_x\text{O}_7$ sample was determined and shown in Figure 5 as a function of temperature. Despite the high Seebeck coefficients (190 - 389 $\mu\text{V/K}$) exhibited by all the compositions, the PF remained very low ($< 20 \mu\text{W/K}^2\cdot\text{m}$), due to the low σ ($\leq 2.0 \text{ S/cm}$). However, the results obtained showed that the power factors of the Nb-doped compositions ($0.05 \leq x \leq 0.25$) were higher than that of undoped composition ($x = 0.00$) in all the measured temperature range, due to the enhanced electrical conductivity. $x = 0.10$ showed a higher PF value especially at high temperatures (773-973 K) than other compositions and recorded the maximum PF value of $\sim 18 \mu\text{W/K}^2\cdot\text{m}$ at 973 K.

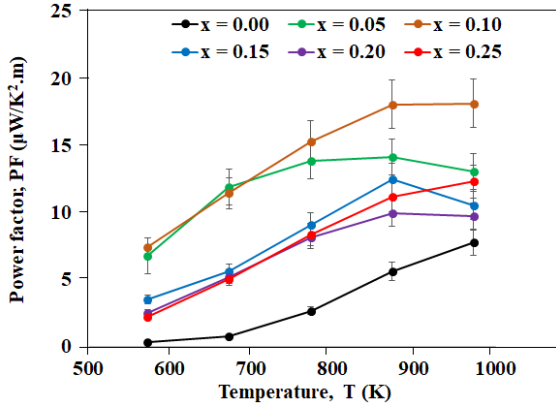


Figure 5. Temperature dependence of power factor for pure and Nb-doped $\text{La}_2\text{Ti}_2\text{O}_7$ ceramics sintered 6 hours in 5% H_2/N_2 at 1773 K.

The temperature dependence of the total thermal conductivity, k and the electronic thermal conductivity, k_E of all samples are shown in Figures 6. The thermal transport behaviour particularly k of the Nb-doped ceramics is irregular with temperature. This behaviour could be related to the complex interplay of phonon scattering including U and N-processes on the ceramic material. Since cation doping of a material increases the grain size thereby promoting carrier (electron) mobility, it could be assumed that phonon propagation as well occurs. As a result, the Nb-doped $\text{La}_2\text{Ti}_2\text{O}_7$ ceramics exhibited a metallic conduction behaviour, which is evidenced in the increased σ and k , respectively.

On the other hand, undoped $\text{La}_2\text{Ti}_2\text{O}_7$ showed the lowest k across the measured temperature range, with a minimum = 1.18 W/m.K at 773-873 K. The reduced relative density observed in $\text{La}_2\text{Ti}_2\text{O}_7$ ceramics indicates an increase in porosity in the microstructure, which significantly affected thermal conductivity. The relation between the k and volume of pores is given in the following equation [36]:

$$k = k_0 \left(1 - P^{\frac{2}{3}}\right) \quad (3)$$

where k_0 is the thermal conductivity of the material without porosity and P is the fraction of pores in the material. The implication of equation 3 therefore, is that increase porosity leads to an increase in phonon scattering, resulting in reduction of k . The minimal k value (1.18 W/m.K) obtained in an undoped $\text{La}_2\text{Ti}_2\text{O}_7$ is lower than the value (1.3 W/m.K at 573 K) obtained in the literature for pure $\text{La}_2\text{Ti}_2\text{O}_7$ [14] and comparable to related polycrystalline PLS compounds such as $\text{Bi}_4\text{Ti}_3\text{O}_{12}$ ($k \sim 1\text{W/m.K}$) [14, 37] and $\text{Sr}_2\text{Nb}_2\text{O}_7$ ($k = 1.5\text{ W/m.K}$) [14, 38]. For the Nb-doped $\text{La}_2\text{Ti}_2\text{O}_7$ compositions reported in this study, $x = 0.10$ showed the highest k value (2.26 W/m. K) at 973 K, while $x = 0.05$

exhibited the lowest k value of 1.49 W/m.K at 773 K, attributed to its large unit cell, large atomic mass, crystal anisotropy and complex crystal structure [37, 38].

The electronic thermal conductivity of all LTO compositions showed similar temperature dependence with σ and increased with increase in temperature as presented in Figure 6(b). From the small k_E values (≤ 0.0044 W/m.K), it is obvious to state that electronic thermal conductivity makes a very small contribution to the total thermal conductivity. This means that k comes mainly from their lattice thermal conductivity [14, 39].

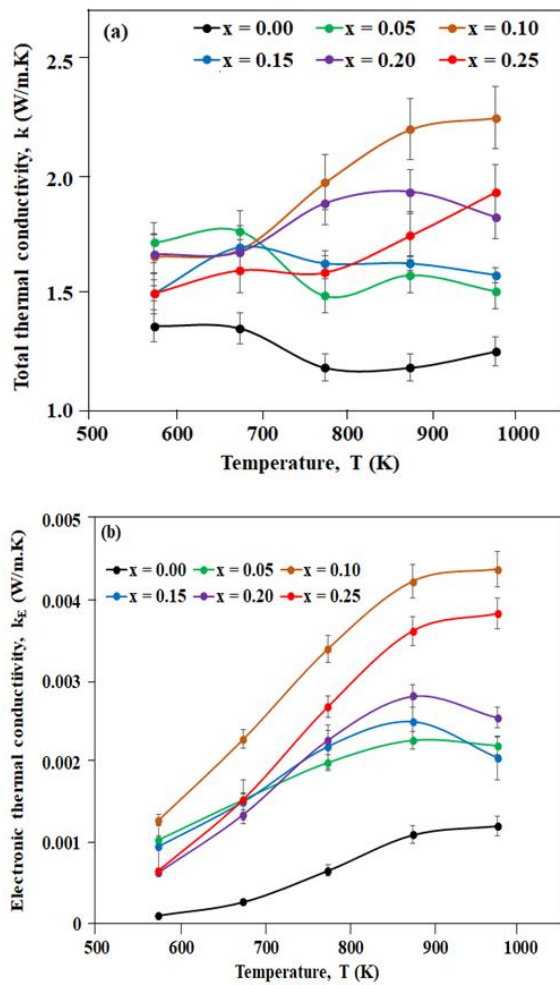


Figure 6. Temperature dependence of (a) total thermal conductivity (b) electronic thermal conductivity for pure and Nb-doped $\text{La}_2\text{Ti}_2\text{O}_7$ ceramics sintered 6 hours in 5% H_2/N_2 at 1773 K.

The cumulative impact of the electrical and thermal transport properties on the thermoelectric performance is illustrated by the temperature dependence of the dimensionless figure of merit, ZT as

shown in Figure 7. From 573 K up to 873 K (573-873 K), $x = 0.00$ (pure $\text{La}_2\text{Ti}_2\text{O}_7$) had the lowest ZT values (≤ 0.0045) because of the low electrical conductivity. The combination of a higher σ and S resulted in a relatively high ZT in Nb-doped $\text{La}_2\text{Ti}_2\text{O}_7$ ceramics compared to undoped $\text{La}_2\text{Ti}_2\text{O}_7$. This suggests that the ZT of $\text{La}_2\text{Ti}_2\text{O}_7$ could be increased by a careful tuning with an appropriate dopant such as Nb. The ZT of all the compositions except $x = 0.15$ increased with increasing temperature within the measured temperature range. The ZT of $\text{La}_2\text{Ti}_{1.85}\text{Nb}_{0.15}\text{O}_7$ ($x = 0.15$) ceramic increased with temperature up to 873 K and decreased at 973 K. Furthermore, in all compositions, $x = 0.05$ and 0.10 showed a high ZT values at low temperatures (573-673 K), and beyond 673 K, $x = 0.05$ exhibited the highest values with a maximum ZT of 0.0084 at 973 K. The highest ZT displayed by 5 mol% Nb-doped $\text{La}_2\text{Ti}_2\text{O}_7$ is traceable to the lowest k value recorded at high temperatures (773-973 K) compared to other Nb-doped $\text{La}_2\text{Ti}_2\text{O}_7$ ceramics.

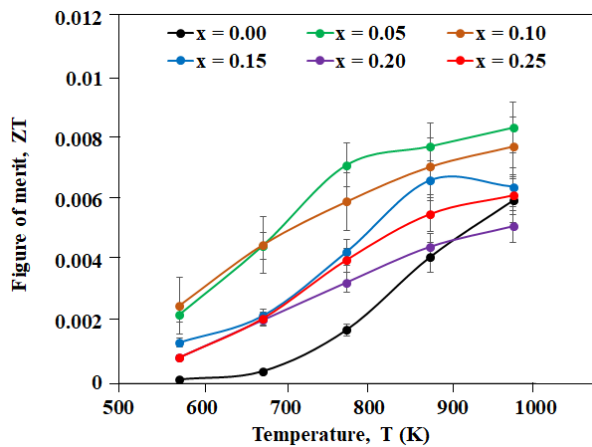


Figure 7. Temperature dependence of figure of merit for pure and Nb-doped $\text{La}_2\text{Ti}_2\text{O}_7$ ceramics sintered 6 hours in 5% H_2/N_2 at 1773 K.

1. CONCLUSIONS

Reduced Nb-doped $\text{La}_2\text{Ti}_2\text{O}_7$ ceramics were studied. The pure $\text{La}_2\text{Ti}_2\text{O}_7$ ceramics exhibited the lowest k (1.18 W/m.K) at 773 – 873 K and the maximum Seebeck coefficient, S (389 $\mu\text{V}/\text{K}$ at 973 K). All doped compositions showed an increase in σ and k , attributed to metallic behaviour due to an increase in carrier concentration and creation of oxygen vacancies. $x = 0.10$ showed the highest PF (18 $\mu\text{W}/\text{K}^2\cdot\text{m}$) at 973 K, resulting from its high electrical conductivity ($\sigma_{\text{max}} = 0.2 \text{ S}/\text{cm}$ at 873 K) and moderate S . The highest ZT (0.0084) was recorded in $x = 0.05$ compositions at 973 K

Comment [pp1]: wrong numbering. Must be corrected to 4

partially due to its low k value. Generally, Nb-doped $\text{La}_2\text{Ti}_2\text{O}_7$ ceramics exhibited very low TE properties especially σ , PF and ZT which are not suitable for thermoelectric applications. However, the high S ($\geq 190 \mu\text{V/K}$) and low k ($\leq 2.26 \text{ W/m.K}$) recorded is a manifestation of the TE potential of Nb-doped $\text{La}_2\text{Ti}_2\text{O}_7$ ceramics.

REFERENCES

- [1] Robert Freer, Anthony V. Powell, Realising the potential of thermoelectric technology: a roadmap. *J. Mater. Chem. C* 2020, **8**: 441.
- [2] Snyder G J , Toberer E S, Complex thermoelectric materials, *Nat Mater* 2008, **7**: 105–114.
- [3] Abanti Nag, Shubha V, Oxide thermoelectric materials: a structure-property relationship, *J. Electron. Mater* 2014, **43**: 962 – 977.
- [4] Terry M. Tritt, Subramanian M, Thermoelectric materials, phenomena and applications: a bird's eye view, *MRS Bull* 2006, **31**: 188 – 198.
- [5] Zhiting Tian, Lee S, Chen G, A comprehensive review of heat transfer in thermoelectric materials and devices, *Annu. Rev. Heat Transf* 2014, **1** -64.
- [6] Gregor Kieslich, Giacomo Cerretti, Igor Veremchuk, *et al* , A chemists view: metal oxides with adaptive structures for thermoelectric applications, *Phys. Status Solidi Appl. Mater. Sci.* 2016, **213**:808–823.
- [7] Jarman T. Jarman, Essam E. Khalil, Elsayed Khalaf, Energy Analyses of Thermoelectric Renewable Energy Sources, *Open J. Energy Effic.* 2013, **2**: 143–153.
- [8] Ichiro Terasaki, Layered Cobalt Oxides: Correlated Electrons for Thermoelectrics,” in *Thermoelectric Nanomaterials: Materials Design and Applications.*, K. Koumoto and T. Mori, (Eds). Berlin Heidelberg: Springer, Springer Series in Materials Science 2013, **182**: 51–70.
- [9] Ryoji Funahashi, Oxide thermoelectric power generation, in 2009 thermoelectric applications workshop, San Diego, CA, September 29 – October 1, 2009. Retrieved from <https://www.energy.gov/eere/vehicles/2009-thermoelectric-applications-workshop-1>
- [10] Petr Tomeš, Matthias Trottman, Clemens Suter, *et al* , Thermoelectric oxide modules (TOMs) for the direct conversion of simulated solar radiation into electrical energy, *Materials (Basel)* 2010,**3**:2801–2814.
- [11] I. Terasaki, Y. Sasago, K. Uchinokura, Large thermoelectric power in NaCo_2O_4 single crystals, *Phys. Rev. B* 1997, **56**: R12685–R12687.
- [12] Yuan Jian Zhong, Feridoon Azough, Robert Freer, The effect of $\text{La}_2\text{Ti}_3\text{O}_9$ second phase on the microstructure and dielectric properties of $\text{La}_2\text{Ti}_2\text{O}_7$ ceramics, *J. Eur. Ceram. Soc.* 1995, **15**: 255–263.

- [13] Sulgiye Park, Maik Lang, Cameron L. Tracy, *et al*, Response of $Gd_2Ti_2O_7$ and $La_2Ti_2O_7$ to swift-heavy ion irradiation and annealing, *Acta Mater* 2015, **93**:1–11.
- [14] Jibran Khaliq, Li Chunchun, Chen Kan, *et al*, Reduced thermal conductivity by nanoscale intergrowths in perovskite like layered structure $La_2Ti_2O_7$,” *J. Appl. Phys* 2015, **117**: 2–8.
- [15] Zhang N, Li Q. J, Huang S.G, *et al*, Dielectric relaxations in multiferroic $La_2Ti_2O_7$ ceramics, *J. Alloys Compd* 2015, **652**: 1–8.
- [16] Sadequa J. Patwe, Vasundhara Katari, Nilesh P. Salke, *et al*, Structural and electrical properties of layered perovskite type $Pr_2Ti_2O_7$: experimental and theoretical investigations, *J. Mater. Chem. C* 2015, **3**: 4570–4584.
- [17] Tanguy Pussacq, Houria Kabbour, Silviu Colis, *et al*, Reduction of $Ln_2Ti_2O_7$ Layered Perovskites: A Survey of the Anionic Lattice, Electronic Features, and Potentials, *Chem. Mater* 2017, **29**: 1047–1057.
- [18] Junying Zhang, Wenqiang Dang, Zhimin Ao, *et al*, Band gap narrowing in nitrogen-doped $La_2Ti_2O_7$ predicted by density-functional theory calculations, *Phys. Chem. Chem. Phys* 2015, **17**: 8994–9000.
- [19] Boston R, Schmidt W. L, Lewin G. D, *et al*, Protocols for the fabrication, characterization, and optimization of n-type thermoelectric ceramic oxides, *Chem. Mater* 2017, **29**: 265–280.
- [20] Fawcett T. G, Needham F, Crowder C.E, Kabekkodu S, Advanced Materials Analysis using the Powder Diffraction File, in *10th National Conference on x-ray Diffraction and ICDD Workshop*, 2009, 1–3.
- [21] Adindu C. Iyasara, Whitney L. Schmidt, Rebecca Boston, *et al*, La and Sm co-doped $SrTiO_{3-\delta}$ thermoelectric ceramics, *Mater. Today Proc* 2017, **4**:12360–12367.
- [22] Elizabeth J. Harvey, Sharon E. Ashbrook, Gregory R. Lumpkin, Simon A. T. Redfern, Characterisation of the $(Y_{1-x}La_x)_2Ti_2O_7$ system by powder diffraction and nuclear magnetic resonance methods, *J. Mater. Chem* 2006, **16**:4665–4674.
- [23] Chang Sun Park, Min Hee Hong, Hyung Hee Cho, Hyung Ho Park, Effect of mesoporous structure on the Seebeck coefficient and electrical properties of $SrTi_{0.8}Nb_{0.2}O_3$, *Appl. Surf. Sci* 2017, **409**:17–21.
- [24] Min Hee Hong, Chang Sun Park, Sangwoo Shin, *et al*, Effect of surfactant concentration variation on the thermoelectric properties of mesoporous ZnO, *J. Nanomater* 2013, **2013**:1–6.
- [25] Peng Peng Shang, Bo Ping Zhang, Yong Liu, *et al*, Preparation and thermoelectric properties of La-doped $SrTiO_3$ ceramics, *J. Electron. Mater* 2011, **40**:926–931.
- [26] Iqbal Mahmud, Man-Soon Yoon, Il-Ho Kim, *et al*, Thermoelectric properties of the ceramic oxide $Sr_{1-x}La_xTiO_3$, *J. Korean Phys. Soc* 2016, **68**:35–40.
- [27] Sudireddy B. R, Agersted K, Sintering and electrical characterization of La and Nb Co-doped $SrTiO_3$ electrode materials for solid oxide cell applications, *Fuel Cells* 2014, **14**: 961–965.
- [28] Peng Peng Shang, Bo Ping Zhang, Jing Feng Li, Ning Ma, Effect of sintering temperature on thermoelectric properties of La-doped $SrTiO_3$ ceramics prepared by sol-gel process and spark plasma sintering, *Solid State Sci* 2010, **12**:1341–1346.

- [29] Venkatasubramanian R, Siivola E, Colpitts T, O'Quinn B, Thin-film thermoelectric devices with high room-temperature figures of merit, *Nature* 2001, **413**:597–602, 2001.
- [30] Jiao Han, Qiu Sun, Ying Song, Enhanced thermoelectric properties of La and Dy co-doped, Sr-deficient SrTiO₃ ceramics, *J. Alloys Compd* 2017, **705**: 22–27.
- [31] A.F. Ioffe, *Semiconductor thermoelements and thermoelectric cooling*. Infosearch Ltd, 1957.
- [32] Hong Chao Wang, Chun Lei Wang, Wen Bin Su, *et al*, Doping effect of La and Dy on the thermoelectric properties of SrTiO₃, *J. Am. Ceram. Soc* 2011, **94**:838–842, 2011.
- [33] Jun Wang, Bo Yu Zhang, Hui Jun Kang, *et al*, Record high thermoelectric performance in bulk SrTiO₃ via nano-scale modulation doping, *Nano Energy* 2017, **35**:387–395.
- [34] Wang H C, Wang C L, Su W B, J Liu, *et al*, Enhancement of thermoelectric figure of merit by doping Dy in La_{0.1}Sr_{0.9}TiO₃ ceramic, *Mater. Res. Bull* 2010, **45**: 809–812.
- [35] Liu J, Wang C L, Li Y, *et al*, Influence of rare earth doping on thermoelectric properties of SrTiO₃ ceramics, *J. Appl. Phys* 2013, **114**.
- [36] Sung-Hwan Bae, Jun-Young Cho, O-Jong Kwon, *et al*, The effect of grain size and density on the thermoelectric properties of Bi₂Te₃-PbTe compounds, *J. Electron. Mater.* 2013, **42**:3390–3396.
- [37] Yang Shen, David R. Clarke, Paul A. Fuierer, Anisotropic thermal conductivity of the Aurivillius phase, bismuth titanate (Bi₄Ti₃O₁₂): a natural nanostructured superlattice, *Appl. Phys. Lett.* 2008, **93**: 10–13.
- [38] Taylor D. Sparks, Paul A. Fuierer, David R. Clarke, Anisotropic thermal diffusivity and conductivity of La-doped strontium niobate Sr₂Nb₂O₇, *J. Am. Ceram. Soc.* 2010, **93**: 1136–1141.
- [39] Shingo Ohta, Takashi Nomura, Hiromichi Ohta, Kunihito Koumoto, High-temperature carrier transport and thermoelectric properties of heavily La- or Nb-doped SrTiO₃ single crystals, *J. Appl. Phys* 2005, **97**: 0341061- 0341064.